# Modeling the effect of temperature on membrane response of light stimulation in optogenetically-targeted neurons

**Helton Maia Peixoto** [1], **Rossana Moreno** [1], **Thiago Moulin** [1], **Richardson N Leão** Corresp. [1]

[1] Brain Institute, Universidade Federal do Rio Grande do Norte

Corresponding Author: Richardson N Leão
Email address: richardson.leao@neuro.ufrn.br

Optogenetics is revolutionizing neuroscience but an often neglected effect of light stimulation of the brain is the generation of heat. In extreme cases, light-generated heat kills neurons but mild temperature changes alter neuronal function. In this work, we investigated heat transfer in brain tissue for common optogenetic protocols using the finite element method. We then modeled channelrhodopsin-2 in a single- and a spontaneous-firing neuron to explore the effect of heat in light stimulated neurons. We found that, at commonly used intensities, laser radiation considerably increases the temperature in the surrounding tissue. This effect alters action potential size and shape and cause increase in spontaneous firing frequency in a neuron model. However, the shortening of activation time constants generated by heat in the single firing neuron model produce AP failures in response to light stimulation. We also found changes in the power spectrum density and a reduction in the time required for synchronization in an interneuron network model of gamma oscillations. Our findings indicate that light stimulation with intensities used in optogenetic experiments may affect neuronal function not only by direct excitation of light sensitive ion channels and/or pumps but also by generating heat. This approach serves as a guide to design optogenetic experiments that minimize the role of tissue heating in the experimental outcome.

# Modeling the effect of temperature on membrane response of light stimulation in optogenetically-targeted neurons

**Helton Maia Peixoto[1,2], Rossana Moreno Santa Cruz[1,3], Thiago C Moulin[4] & Richardson Naves Leão[1,2,*]**

1. Neurodynamics Lab, Brain Institute, Federal University of Rio Grande do Norte, Natal - RN, Brazil
2. Developmental Genetics Unit, Department of Neuroscience, Uppsala University, Husarg 3, 75237, Uppsala, Sweden
3. Federal Institute of Education, Science and Technology of Paraiba, 58015-430, João Pessoa - PB, Brazil
4. Institute of Medical Biochemistry, Federal University of Rio de Janeiro, Cidade Universitária 21044-020, Rio de Janeiro/RJ, Brazil.

Corresponding Author:
Richardson N. Leão
Address: Brain Institute, Av. Nascimento de Castro, 2155 – Lagoa Nova, Natal - RN, 59056-450, Brazil.
Phone: +558432154592
E-mail: richardson.leao@neuro.ufrn.br

## ABSTRACT

Optogenetics is revolutionizing neuroscience but an often neglected effect of light stimulation of the brain is the generation of heat. In extreme cases, light-generated heat kills neurons but mild temperature changes alter neuronal function. In this work, we investigated heat transfer in brain tissue for common optogenetic protocols using the finite element method. We then modeled channelrhodopsin-2 in a single- and a spontaneous-firing neuron to explore the effect of heat in light stimulated neurons. We found that, at commonly used intensities, laser radiation considerably increases the temperature in the surrounding tissue. This effect alters action potential size and shape and cause increase in spontaneous firing frequency in a neuron model. However, the shortening of activation time constants generated by heat in the single firing neuron model produce AP failures in response to light stimulation. We also found changes in the power spectrum density and a reduction in the time required for synchronization in an interneuron network model of gamma oscillations. Our findings indicate that light stimulation with intensities used in optogenetic experiments may affect neuronal function not only by direct excitation of light sensitive ion channels and/or pumps but also by generating heat. This

approach serves as a guide to design optogenetic experiments that minimize the role of tissue heating in the experimental outcome.

## INTRODUCTION

Optogenetics refers to a group of techniques that rely on genetics and optics for the deterministic control or study of (generally excitable) cells from a similar genetic background (Fenno, Yizhar & Deisseroth, 2011). The radical idea of using light-driven ion channels and pumps from unicellular organisms to modulate neurons was pioneered by Deisseroth, Nagel and Boyden and has now spread to neuroscience laboratories throughout the world (Knöpfel et al., 2010; Fenno, Yizhar & Deisseroth, 2011). Limiting factors of the technique include the availability of genetic markers (Lerchner et al., 2014), the invasiveness of the gene delivery and specially difficulties of delivering light throughout large brain volumes (Lerchner et al., 2014). Perhaps for these reasons, optogenetics studies are vastly more common in small animals, especially mice and rats (Aravanis et al., 2007; Madisen et al., 2012). Optogenetics also covers the ability of probing neural activity using designed genetic fluorescent voltage or calcium sensors (Knöpfel et al., 2010). These applications involve the detection of neural activity using genetic probes by complex hardware (for acquiring photon emission) and the usage of very stable and powerful light sources for fluorescence excitation, particularly, in *in vivo* experiments, in which autofluorescence of blood and movement artefacts generates larger alterations in fluorescence than the neural activity of study (Akemann et al., 2010).

To date, most *in vivo* experiments rely on light stimulation of neural tissue using fibre-coupled lasers of various wavelengths. In general, blue lasers are used for exciting neurons expressing light-activated ion channels (channelrhodopsin and its variants) and yellow/green lasers are used for neurons expressing light-activated chlorine or proton pumps (halorhodopsin or archaerhodopsin, respectively). Due to poor penetration of blue and yellow light in the brain, high laser power and/or fibres of high numerical aperture are often used to achieve functional stimulation of deep brain regions (Adamantidis et al., 2014; Adelsberger et al., 2014). Hence, brain tissue is irradiated with high light power that can be deleterious to neuronal function but surprisingly little attention has been paid on effects of light stimulation itself in optogenetic experiments. Absorbed light generates heat that can lead to permanent tissue damage. Additionally, neuronal excitability is acutely affected by temperature through the changes in Nernst equilibrium potential and by altering the gating properties of ion channels (Andersen & Moser, 1995; Kim & Connors, 2012). Thus, light alone can generate effects in neuronal function

that are unrelated to the genuine 'optogenetic effect'. In modeling studies, an empirical factor ($Q_{10}$) is used to multiply rate constants in order to add temperature dependence to the classical Hodgkin and Huxley formalism (Fitzhugh, 1966).

Fibre-optics-delivered light in biological tissues is partially reflected at the fibre–tissue interface and partially transmitted through the tissue. Absorbed light is converted to heat, radiated in the form of fluorescence and/or consumed in photobiochemical reactions. The time-dependent heat production in brain tissue can be described by the bio-heat equation (Pennes, 1948), in which changes in tissue temperature can be calculated in time and space. These equations can also account for the buffering of temperature by blood perfusion. Furthermore, laser radiation increases stored energy that results in the diffusion of heat away from the irradiated area in proportion to the temperature gradients generated within the tissue (Welch & van Gemert, 2011). Therefore, the conclusion drawn from optogenetic experiments may be hindered if the direct heat effect of light stimulation is not accounted for.

In this work, we modelled the optothermal effect in mice brain tissue produced by visible light laser sources (with a Gaussian profile) in both continuous and pulsed modes (Aravanis et al., 2007; Bernstein et al., 2008) in order to understand how heat can affect the transfer function of single neurons and how it can alter their response to photocurrents. We first approached the time/space numerical solution of Pennes' bio-heat equation comprising the effects of blood perfusion and metabolism with the finite element method (FEM) (Zimmerman, 2004). We then simulated the effect of varying heat in two single neuron models (Wang & Buzsáki, 1996; Rothman & Manis, 2003) that include a voltage and light dependent current based on the channelrhodopsin 2 dynamics (Williams et al., 2013) to demonstrate that heat itself can considerably alter neuronal dynamics.

## MATERIALS & METHODS

*Scattering and absorption*

A source of scattering in biological tissues is the difference of refractive indices between subcellular organelles and the surrounding cytoplasm. In this case, a part of the incident light is redirected over a range of angles relative to the scattering particle. In biomedical photonics, scattering processes are important in both diagnostic and therapeutic applications (Vo-Dinh, 2003; Welch & van Gemert, 2011).

Scattering can be described by assuming the incident light as a wave of uniform amplitude in any plane perpendicular to the direction of propagation — a plane wave. For a monochromatic plane wave propagating in a medium and colliding with a scattering object, some amount of power gets spatially redirected. The ratio of the power (energy per second) scattered out of the plane wave to the incident intensity (energy per second per area) is the scattering cross section, $\sigma_s$, in $m^2$, given by (Vo-Dinh, 2003, p.; Welch & van Gemert, 2011):

$$\sigma_s(\hat{s}) = \frac{P_s}{I_w}, \quad (1)$$

where, $\hat{s}$ is the propagation direction of the plane wave relative to the scatterer, $P_s$ is the power scattered and $I_w$ is the intensity of the wave. The scattering cross section is equivalent to the area that an object withdraws from the uniform plane wave in order to remove the observed amount of scattered power.

The scattering coefficient, $\mu_s$, characterizes the distribution of scatterers in a medium, and is a function of the scattering cross section:

$$\mu_s = \rho_s \sigma_s, \quad (2)$$

in which, $\rho_s$ represents the numeric density ($m^{-3}$) of the scatterers. The scattering coefficient is essentially the scattering cross section per unit volume of medium.

Absorption is a process involving the extraction of energy from light by a molecular species. It is also important in diagnostic and therapeutic applications in biomedical photonics. The concept of cross section is also used for absorption, where the power absorbed is part of the incident intensity. Therefore, for a given absorber, the absorption cross section, $\sigma_a$, can be defined as:

$$\sigma_a(\hat{a}) = \frac{P_a}{I_w}, \quad (3)$$

here, $\hat{a}$ is the propagation direction of the plane wave relative to the absorber, $P_a$ is the power absorbed and $I_w$ is the intensity of the wave. Similarly, a medium with absorbing particles can be characterized by the *absorption coefficient*, $\mu_a$:

$$\mu_a = \rho_a \sigma_a \,, \tag{4}$$

where, $\rho_a$ represents the numeric density ($m^{-3}$) of the absorbers.

*Reflection and refraction*

It is common to define the refractive index of a medium, $n$, in terms of the phase velocity, $v_f$, of light in the referred medium (Sadiku, 2010; Balanis, 2012; Peatross & Ware, 2015):

$$n = \frac{c}{v_f} \,, \tag{5}$$

in which, $c = 3 \cdot 10^8$ m/s is the speed of light in vacuum and $n_{vac} = 1$. The wavelength of light changes during the propagation from one medium to another. Interestingly, the light frequency, $f$ (Hz), does not change. The wavelength of light in a medium, $\lambda_m$, is given as a function of the wavelength of light in vacuum, $\lambda$ (m) (Vo-Dinh, 2003):

$$\lambda_m = \frac{\lambda}{n} \,. \tag{6}$$

Reflection and refraction occur when an electromagnetic wave propagates from a medium with a given refractive index to a medium with a different index. The amount of energy reflected by and transmitted through the boundary depends not only on the refractive indices, but also on the angle of incidence and the polarization of the incoming wave (Vo-Dinh, 2003).

Considering a normal wave incidence onto a planar boundary, the fraction of the incident energy that is reflected is given by the reflection coefficient ($R$), in this case expressed as a function of the relative refractive indices of the tissue, $n_t$, and the surrounding media, $n_1$:

$$R = \left( \frac{n_1 - n_t}{n_1 + n_t} \right)^2 . \tag{7}$$

The relation between the angle of incidence, $\theta_1$, and the angle of refraction, $\theta_2$, for the transmitted light is given by Snell's law (Balanis, 2012; Peatross & Ware, 2015):

$$\sin(\theta_2) = \frac{n_1}{n_2} sin(\theta_1) \,. \tag{8}$$

Similarly, the relation between the incident wavelength (medium 1) and the refracted wavelength (medium 2) can be obtained by (Vo-Dinh, 2003, p.):

$$\lambda_2 = \frac{n_1}{n_2}\lambda_1 . \quad (9)$$

*Photon flux*

Since light frequency does not depend on the refractive index, the photon energy is always the same as in the vacuum, according to (Vo-Dinh, 2003; Welch & van Gemert, 2011):

$$E = hf , \quad (10)$$

where, $h$ = 6.626·10$^{-34}$ Js is Planck's constant and $f$ is the frequency (Hz).

The photon flux in a laser light beam is defined as the total number of photons crossing a particular section of the light beam, per unit area and per unit time (Orazio, 2010). The number of photons emitted per second is given by:

$$N_p = P\frac{\lambda}{hc}, \quad (11)$$

in which, $P$ is the laser power. Then, the photon flux, $\phi_p$, can be obtained as a function of the cross section area ($A$, m$^2$) of the light beam as well as the intensity ($I$, W/m$^2$) of the light beam, according to (Orazio, 2010):

$$\phi_p = \frac{P\,\lambda}{Ahc} = I\frac{\lambda}{hc}. \quad (12)$$

*Gaussian laser beam*

Assuming that a laser beam with irradiance profile $\vec{E}(x,y)$ is incident upon the tissue, the beam in the $z$ direction attenuates exponentially with the distance $d$ in the tissue (Welch & van Gemert, 2011). The irradiance can be defined as the radiant energy flux incident on a point of the surface, divided by the area of the surface. Many laser sources emit beams that approximate a Gaussian profile, in which case the propagation mode of the beam is the fundamental transverse

electromagnetic mode ($TEM_{00}$). A transverse mode of an electromagnetic radiation is a particular electromagnetic field pattern measured in a plane perpendicular to the propagation direction of the beam. In the case of a TEM mode, both electric and magnetic fields are normal to the direction of the propagating light. The mathematical function that describes the Gaussian beam is a solution to the paraxial form of the Helmholtz equation (Sadiku, 2010; Balanis, 2012).

The solution, in the form of a Gaussian function, represents the complex amplitude of the electric and magnetic fields of the beam. The electric and magnetic fields together propagate as an electromagnetic wave. A representation of just one of the two fields is sufficient to describe the properties of the beam (Orazio, 2010). In this way, let us assume the beam originates in the plane $z = 0$ and propagates along the positive $z$-axis. If we also assume the free-space optical field at any point along the propagation path is symmetric, then it can be expressed as a function of $r = \sqrt{x^2 + y^2}$ and $z$, considering $r$ as the radial distance from the beam center line. Thus, the reduced wave equation for the electric field in cylindrical coordinates, $\vec{E}(r,z)$ can be written as (Orazio, 2010):

$$\frac{1}{r}\frac{\partial}{\partial r}\left(r\frac{\partial \vec{E}}{\partial r}\right) + \frac{\partial^2 \vec{E}}{\partial z^2} + k^2\vec{E} = 0\,, \tag{13}$$

where, $k = \frac{2\pi}{\lambda}$ is the wave number (rad/m). The propagation in free space of the $TEM_{00}$ lowest-order mode assumes that the transmitting aperture of the beam is located in the plane $z = 0$, and the amplitude distribution, $a_0$ $(W/m^2)^{1/2}$, located on the optical axis ($r = 0$), is Gaussian with effective beam radius (spot size) $W_0$ (m), where $W_0$ denotes the radius at which the field amplitude falls to $1/e$ of that on the beam axis. The expression for the electric field of a Gaussian beam propagating the $TEM_{00}$ lowest-order mode (Andrews & Philips, 2005) is given by:

$$\vec{E}(r,0) = a_0 exp\left(-\frac{r^2}{{W_0}^2} - \frac{ikr^2}{2F_0}\right), \tag{14}$$

in which, $F_0$ is the beam radius of curvature (m). The amplitude, $A_0$, and the phase, $\varphi_0$, of a Gaussian beam wave can be obtained by (Andrews & Philips, 2005):

$$A_0 = a_0 exp\left(-\frac{r^2}{{W_0}^2}\right), \quad (15)$$

$$\varphi_0 = -\frac{kr^2}{2F_0}. \quad (16)$$

Gaussian functions can assume multi-dimensional forms by composing the exponential function with a concave quadratic function (Weisstein, 2016). A particular example of a two-dimensional Gaussian function, in the *x*-*y* plane, is:

$$f(x,y) = A\ exp\left[-\left(\frac{(x-x_0)^2}{2\sigma_x^2} + \frac{(y-y_0)^2}{2\sigma_y^2}\right)\right]. \quad (17)$$

Considering a bell curve shape for the Gaussian function, the parameter *A* is the maximum amplitude of the curve; $x_0$ and $y_0$ are the center position of the curve in *x* and *y* axis; $\sigma_x$ and $\sigma_y$ are the *x* and *y* spreads or standard deviations of the Gaussian curve.

*Light propagation in brain tissue*

*In vitro* and *in vivo* optogenetic experiments commonly use laser sources and optical fibres to delivery light to the tissue in an accurate and efficient manner. The setup is relatively simple and consists of laser sources coupled to optical fibres to reach the region of interest (ROI) in the tissue. *In vivo* experiments in deep regions of the brain, for example, also require a stereotactic surgery to position the tip of the optical fibre in the ROI into the brain (Zhang et al., 2015). Depending on the distance from the fibre tip and the optical properties of the surrounding tissue, the emitted light can propagate with uneven intensity.

Light intensity *I*, in mW/mm$^2$, from the fibre tip to a distance *d* (*z* direction), in mm, in the brain can be calculated using Kubelka-Munk (K–M) model for diffuse media (Yang & Miklavcic, 2005; Dzimbeg-Malcic, Barbarić-Mikočević & Itrić, 2010). This model consists of a set of differential equations that describe the fact that the light beam traveling in the transmitted direction decreases in intensity due to absorption and scattering, and gains intensity from the scattering that occurs in the beam arising from other directions. Therefore, they provide the foundations for many quantitative studies of absorption and scattering for a planar, homogeneous and ideally diffuser medium, illuminated on one side by a monochromatic light source.

The transmittance ($T$) is the relationship between the light intensity measured in the tissue at a distance $d$ and the light intensity measured without tissue, $\frac{I(d)}{I(d=0)}$, considering both scattering and absorption effects and is given by (Vo-Dinh, 2003):

$$T = \frac{b}{a\sinh(bd\mu_s) + b\cosh(bd\mu_s)}, \quad (18)$$

in which, $\mu_s$ can be given in mm$^{-1}$ (Aravanis et al., 2007; Bernstein et al., 2008), $d$ is the distance in the brain tissue in mm, and $a$ and $b$ are given by (Vo-Dinh, 2003):

$$a = 1 + \frac{\mu_a}{\mu_s}, \quad (19)$$

$$b = \sqrt{(a^2 - 1)}, \quad (20)$$

here, $\mu_a$ can also be given in mm$^{-1}$ (Aravanis et al., 2007; Bernstein et al., 2008).

Light intensity can be estimated by the product between the transmittance ($T$) and the geometric loss ($g_{loss}$) due to light dispersion in the tissue. The geometric loss is obtained by the decrease in light intensity due to the conical shape observed from the fibre tip ($d$ = 0) to a certain distance ($d$) in the tissue. The divergence angle ($\theta_{div}$), for a multimode fibre, is given by (Aravanis et al., 2007):

$$\theta_{div} = sin^{-1}\left(\frac{NA_{fib}}{n_t}\right), \quad (21)$$

where, $n_t$ is the refractive index of the tissue and $NA_{fib}$ is the numerical aperture of the optical fibre. Considering the conservation of energy, we can calculate the geometric loss ($g_{loss}$) to a given distance ($d$) in the tissue as (Aravanis et al., 2007):

$$g_{loss} = \frac{\rho^2}{(d+\rho)^2}, \quad (22)$$

with,

$$\rho = r\sqrt{\left(\frac{n_t}{NA_{fib}}\right)^2 - 1}\,, \tag{23}$$

in which, $r$ is the fibre core radius. In this way, the expression for the normalized light intensity ($I_N$), considering scattering, absorption and geometric loss is given by:

$$I_N = \frac{I(d)}{I(d=0)} = g_{loss} \cdot T\,. \tag{24}$$

We can consider $I(d = 0)$ as the light intensity at the fibre tip that can be obtained in mW/mm$^2$ simply by:

$$I(d=0) = \frac{P}{A\eta}, \tag{25}$$

where, $P$ is the power emitted by the light source in mW, $A = \pi r^2$ is the area of the optical fibre in mm$^2$, and $\eta$ is the coupling efficiency between the optical fibre and the light source (dimensionless).

Finally, the light intensity in mW/mm$^2$ at a desired region of interest in the tissue, assuming a distance $d$ in mm from the fibre tip, is given by:

$$I(d) = I(d=0) \cdot I_N\,. \tag{26}$$

We used the MATLAB commercial software to simulate scattering and absorption characteristics in mice brain tissue. Table 1 shows the parameters and respective values used for these simulations.

*Heat transfer in mice brain tissue*

Heat is inevitably produced when the propagating light is absorbed by biological tissues. The generated heat can be described by the term, $H_s$, (heat source) proportional to the light intensity at a distance $d$, $I(d)$, and the absorption coefficient, $\mu_a$ (Vo-Dinh, 2003):

$$H_s(d) = \mu_a \cdot I(d)\,. \tag{27}$$

The traditional bio-heat equation describes the change in tissue temperature over time that can be expressed at a distance *d* in the tissue. Furthermore, blood perfusion occurs in living tissues, and the passage of blood modifies the heat transfer in tissues. Pennes (1948) has established a simplified bio-heat transfer model to describe heat transfer in tissue by considering the effects of blood perfusion ($\omega_b$) and metabolism ($H_m$) (Vo-Dinh, 2003; Elwassif et al., 2006):

$$\rho C_p \frac{\partial T}{\partial t} = \nabla(k\nabla T) - \rho_b \omega_b C_b (T - T_b) + H_s + H_m, \quad (28)$$

where, $\rho$ is the tissue density (kg/m$^3$), $C_p$ is the specific heat of the tissue (J/kg°C), $k$ is the thermal conductivity of the tissue (W/m°C), $\rho_b$ is the blood density (kg/m$^3$), $\omega_b$ is the blood perfusion (1/s), $C_b$ is the specific heat of the blood (J/kg°C), $T$ is the temperature of the tissue (°C), $T_b$ is the blood temperature (◦C), $H_s$ is the heat source due to photon absorption (W/m$^3$), and $H_m$ is the term that represents heat generated by metabolism (W/m$^3$).

The interaction between metabolic heat generation and blood perfusion was investigated and it was proved that the temperature increases during Deep Brain Stimulation (DBS) (Elwassif et al., 2006). The metabolic rates can be obtained from the blood perfusion rates in order to maintain the initial brain temperature at 37 °C, as given by (Elwassif et al., 2006):

$$H_m = \rho_b \omega_b C_b (T - T_b). \quad (29)$$

Other environmental interactions that can affect the stored energy include radiation and convection from the sample surface, the loss of vapor phase water from the sample, and convection with blood that is perfused though the vascular network from arterial and venous sources. This network has a very specific geometry that is unique to a tissue or organ and can affect significantly the capability to exchange heat with the tissue in which it is embedded (Welch & van Gemert, 2011).

Additionally, thermal boundary interactions occur over the surface area with the environment and are often characterized as convective and irradiative processes. Laser radiation process increases the stored energy from its initial state and, as a result, it diffuses the heat away from the irradiated area in proportion to the temperature gradients developed in the tissue. A quantitative characterization of the formation of these gradients and the heat flow that they drive are the focus of heat transfer analysis (Welch & van Gemert, 2011).

In the case of convective boundary conditions, heat transfer occurs when a solid substrate is in contact with a fluid at a different temperature (Welch & van Gemert, 2011). The magnitude of the heat exchange can be calculated according to Newton's law of cooling, that describes the convective flow, $H_{conv}$ (W/m$^2$), at the surface in terms of the convective heat transfer coefficient, $h$ (W/m$^2$˚C) and the temperatures of the sample ($T$) and the external environment ($T_{ext}$), in ˚C:

$$H_{conv} = h(T - T_{ext}) . \quad (30)$$

Heating generated within the biological material is governed by the following expression (Yang & Miklavcic, 2005):

$$H(x,y,z) = P(1 - R_F)\frac{\mu_a}{\pi\sigma_x\sigma_y} exp\left[ -\left( \frac{(x - x_0)^2}{2\sigma_x^2} + \frac{(y - y_0)^2}{2\sigma_y^2} \right) \right] exp(-\mu_a z) , \quad (31)$$

in which, the first exponential function represents the two-dimensional Gaussian distribution in *xy*-plane, in accordance to Eq. (17). The second exponential function represents the exponential decay due to absorption (Yang & Miklavcic, 2005).

Some considerations in using Eq. (31) are: the reflection and absorption coefficients are assumed to be constant; the sample is assumed to have a planar surface aligned with the *xy*-plane of the global coordinate system and whose top matches $z = 0$ (distance at the fibre tip); the center of the beam can be easily shifted by changing $x_0$ and $y_0$; the beam width can be easily controlled by the standard deviation parameters $\sigma_x$ and $\sigma_y$.

Heat transfer simulations were performed using COMSOL Multiphysics 4.4 commercial software based on finite element method that is a numerical technique used for approximating partial differential equations (subdomains) to a more complex equation over a larger domain. Laser heating was simulated considering two stationary conditions: continuous mode and pulsed mode. We used a biological material with mice brain tissue characteristics (gray matter). The material properties were assumed to be constant and are shown in Table 2.

*Channelrhodopsin 2 and Neuron models*

We first modeled the effect of temperature alone in a pyramidal cell model and in a network of basket cells known to generate gamma oscillations. We have implemented a single compartment CA1 neuron model described by Migliore (Migliore, 1996). He has implemented a multicompartment model in his original work, but here we only employ the soma with an

inactivating sodium conductance (max. 30 nS), a delayed rectifier $K^+$ conductance (max. 10 nS), conductance from an M current (max. 0.6 nS) and from an H current (max. 0.3 nS). Kinetics for all currents were download from ModelDB (https://senselab.med.yale.edu/modeldb/, Accession:2937).

In addition, we have used the same $Q_{10}$ values for all voltage-gated currents as the original publication (Wang & Buzsáki, 1996). Temperature values from the heat transfer simulation were fed to the neuron model by a 'look up time/temperature table' where each rounded ms value corresponded to a single temperature value. Simulations were run for 90 s (30 s for stabilisation with constant temperature and 60 s with variable temperature). The model was solved in MATLAB using the built-in solver 'ode23'. The interneuron network gamma model was simulate using Neuron with no changing in parameters from the model available from ModelDB (Accession:26997) exception by setting temperature to 37 or 39 $^oC$. These simulations were run for 500 ms with constant temperature. Note that the original study of Wang and Buzsáki did not account for temperature; however, the uploaded model in ModelDB includes $Q_{10}$ for kinetic variables (Wang & Buzsáki, 1996).

Power spectrum density analysis and cross-correlation of action potentials were calculated from spike trains transformed in a series of 0 s (no spike) and 1 s (spike) with 0.1 ms-precision (Hilscher, Leão & Leão, 2013). Power spectral density analysis of binary spike series was performed using the Welch's method ("pwelch" command in MATLAB). Cross-correlograms (CCGs) were calculated as described previously (Hilscher, Leão & Leão, 2013) and then smoothed by a moving average filter with a span of 10 ms (Hilscher, Leão & Leão, 2013). Cross-correlations over a lag range of ±0.1 s. Synchrony index (SI) is defined as the maximum value of the CCG.

We have implemented the channelrhodopsin 2 empirical model (Williams et al., 2013) in two single neuron models to test the interaction of temperature and optocurrents: a single basket cell from Wang and Buzsaki network model (Wang & Buzsáki, 1996) and a anteroventral cochlear nucleus bushy cell model (Rothman & Manis, 2003). The equations and parameters from the neuron models can be found in the original publications (Wang & Buzsáki, 1996; Rothman & Manis, 2003) and equations and parameters for channelrhodopsin optocurrents are found in (Williams et al., 2013). All models were implemented in MATLAB (Mathworks) and the codes can be downloaded from https://github.com/cineguerrilha/Neurodynamics/tree/master/Cell_Models.

## RESULTS

In this work, we have first simulated the heat generated by light absorption in a typical optogenetic experiment (Figure 1a – a diode pumped solid-state – DPSS – laser source coupled to a multimode optical fibre that transmits light directly to deep brain regions (Zhang et al., 2015)). Subsequently, simulated the effect of heat in single neurons and networks. We have also examined the additive effect of heat and light in simulations that included a channelrhodopsin 2 model (Williams et al., 2013). Bioheat transfer was solved numerically using Pennes equation with the finite element method and temporal changes in temperature at a given point in space were applied to a single compartment neuron model (with Hodgkin and Huxley formalism).

We first simulated beam geometry and light dispersion. A DPSS laser emits a Gaussian beam that the propagation mode is the fundamental transversal electromagnetic ($TEM_{00}$) (Figure 1b and c and Eq. (17). Figure 1d shows the normalized geometric light loss due to dispersion in *z*-*y* plane within the tissue as a function of the distance from the fibre tip in *z* direction. The divergence angle is determined by the optical fibre numerical aperture according to Eq. (21). Light speed is altered during propagation because of the difference of refractive indices and their dependence with wavelength. Consequently, the wavelength can change during propagation and this effect is not only observed in the interface between fibre and tissue, but also within the tissue, due to its anisotropic refractive indexes between different brain regions. The wavelength change between two different media, which is calculated using Snell's law (Eq. (8)), is illustrated in Figure 1e. Assuming that light propagates from an optical fibre (medium 1) to the tissue (medium 2), where N is a perpendicular line to the surface of separation between the two media, and considering $n_{1b}$ = 1.4644 as the refractive index of the fibre core at 473 nm, $n_{1y}$ = 1.4587 the refractive index of the fibre core at 593 nm, and $n_2$ = 1.36 the refractive index of the tissue (mouse brain, gray matter), the wavelength shifts for blue (473 nm) and yellow (593 nm) lights due to refraction are 36 nm and 43 nm, respectively (Eq. (9)). Yet small, wavelength shifts have to be considered specially in modelling studies as there is an obvious relationship between wavelength and light absorption in both light-sensitive ion channels and fluorescent proteins (Zhang et al., 2015), even if the photon energy remains the same, once small changes in the wavelength affect the response of the light-sensitive ion channels and fluorescent proteins. After light power at a given point is calculated, photon flux (number of irradiated photons per unit time and per unit area) at that point can be obtained by Eq. (12). Photon flux can then be correlated to photocurrents in channelrhodopsin models (Foutz, Arlow & McIntyre, 2012). Photon flux simulations shown in Figure 1e in which a 20 mW

473 nm laser is pulsed with durations of 15, 60, and 100 ms. The different pulse durations were chosen to ilustrate that the pulse width changes alter the amount of photons passing through a surface.

We then used Kubelka-Munk model to calculate light intensity vs. distance considering absorption (Vo-Dinh, 2003). Light absorption by the tissue has no direct relation to the production of photocurrents by channelrhodopsin; however, absorption produces heat, a side effect of light stimulation (Shapiro et al., 2012). Light absorption also changes (although slightly) the relation between light intensity and tissue depth (Figure 2a). If we assume a threshold of 10 $mW/mm^2$ (green line) is used (Bernstein et al., 2008), the depth for channelrhodopsin-2 activation is 0.39 mm (473 nm) and for halorhodopsin activation is 0.42 mm (593 nm). These simulations indicate that only cells and neurites at the vicinity of the fibre are affected by light stimulation and are in agreement with a previous study (Stujenske, Spellman & Gordon, 2015).

We next computed the production of heat in the tissue caused by light absorption using FEM. For heat transmission simulations, we used a rectangular prism of dimensions equal to 3.5 x 3.5 x 5 ($mm^3$) representing a mouse brain tissue. Optogenetic experiments often use specific stimulation protocols with yellow light to activate halorhodopsin and blue light to activate channelrhodopsin (Cardin et al., 2009; Mikulovic et al., 2016). We, therefore, simulated the interaction between the mouse brain and the yellow light radiation (593 nm wavelength), with the laser source operating in continuous mode, while the blue light radiation (473 nm wavelength) laser source operating in pulsed mode.

Temperature changes at a distance $d$ = 10 μm from the fibre tip caused by continuous light radiation (593 nm) as a function of time are shown in Figure 3a. We simulated heat transfer due to continuous yellow light for different values of power emitted by the laser source: 1, 10, 20, 30, and 40 mW. According to Figure 3a, during the first 5 s, the rate of temperature variation is higher. Thereafter, the temperature continues to increase more slowly moving toward the steady state condition. For light power up to 10 mW, temperature increases about 0.5 ºC. For 20, 30, and 40 mW, the increase in temperature after one minute of radiation is between 1 and 2 ºC. Figure 3b shows a temperature distribution in 3D view, 2D top view ($x$-$y$), and 2D slice center view ($z$-$x$, constant $y$), for continuous yellow light radiation (20 mW and 60 s, indicated by the red asterisk shown in Figure 3a) and pulsed blue light radiation (473 nm), 12 Hz and 18% of duty cycle – percentage of a period in which the light is turned on (black asterisk indicated in Figure 3c). We have also computed temperature changes for 20 mW blue light, at 60 s and 10 μm from the fibre tip, for frequencies varying from 1 to 40 Hz with duty cycles varying from 1%

to 100% (Figure 3c). These results show that lower duty cycles minimizes temperature changes by light stimulation.

Currents produced by voltage-gated ion channels are directly influenced by temperature. It is known for decades that channel opening and closing are generally faster in higher temperatures and conductance/voltage relationship and ion reversal potential are also be affected by temperature (Fitzhugh, 1966). To illustrate the effect of temperature in firing, we used a basket cell model (Wang & Buzsáki, 1996). For these simulations we used two temperatures (37 $^{o}$C and 39 $^{o}$C – the latter can be quickly produced by a pulsed laser at 40 Hz and 90% duty cycle and at 10 μm-distance from the center of the fibre tip – Figure 4). In the model implemented here, action potentials become smaller and briefer with no change in firing threshold (Figure 4a and b). Spontaneous firing frequency of the neuron used in this simulation also increases (Figure 4c). Optogenetics has been used to study the mechanisms behind neuronal synchrony and brain rhythm generation (Cardin et al., 2009). Hence, we further investigated the effect of heat generated by light stimulation itself (rather than photocurrents in channelrhodopsin-expressing neurons) in a network model comprised solely by basket cells that synchronise in gamma frequency (Wang & Buzsáki, 1996). The model is composed of 100 interconnected fast spiking interneurons (same as in Figure 4) (Wang & Buzsáki, 1996). In the Wang and Buzsáki's model (Wang & Buzsáki, 1996), neurons in the network take around 200-300 ms to fire in gamma frequency from a relatively asynchronous onset (Figure 4a and d). If temperature is raised by 2 °C, the network is synchronized in less than 50 ms (Figure 4a and d) from the onset of simulation. Firing frequency of the interneurons in the network also increased by raising the temperature in 2 °C (Figure 4c). This changing in frequency caused a shift in the peak of 'gamma oscillation' in the power spectrum (Figure 4c) Hence, heat itself can theoretically facilitate the generation of oscillations and/or alter their frequency.

We further assess the effect of raising temperature in neuronal synchronization using previously described synchrony metrics (Leao, Leao & Walmsley, 2005; Hilscher, Leão & Leão, 2013). Autocorrelation histograms of all 100 neurons in the model is shown in Figure 5a for 37 °C and at 39 °C. Heating the network model caused neurons to fire at greater rhythmicity (Figure 5a). In addition, cross-correlogram also showed greater synchrony when simulations were executed at 39 °C (compared to 37 °C). This increase in synchrony is reflected by a significant rise in synchronisation coefficient (Figure 5b). The mean synchronisation index (SI) for all possible neuron pair combinations (9900 pairs) was equal to 0.16 for 37 °C and 0.22 for 39 °C. These results show that heating can, not exclusively, change the frequency of brain oscillations but also alter the coordination and synchrony of neuronal firing.

We then combine temperature and radiation in modeled neurons that also contained a channelrhodopsin 2-driven photocurrents (Wang & Buzsáki, 1996; Rothman & Manis, 2003; Williams et al., 2013). We have used two distinct cell models to illustrate the interaction of channelrhodopsin photocurrents with other ionic currents in the neuron. The basket cell shows high frequency firing that increases proportionally to the injected current (Martina et al., 1998) and a bushy cell of the dorsal cochlear nucleus that show single action potentials in response to continuously injected currents (Leao et al., 2006). At 1 mW power, the basket cell model fired action potentials at the beginning of each pulse whether at 37 °C or 39 °C (Figure 6a). However, the bushy cell model only fired APs at physiological temperature (Figure 6a). The tissue reaches 39 °C quickly for duty 50% or 90% duty cycles but temperature only rises mildly for 10% duty cycle (Figure 6b). Nevertheless, even at 10% duty cycle, bushy cell light-elicited AP amplitude is still affected by the small increase in temperature (Figure 6c and d). Taken together, this data suggests that temperature can alter the efficiency of photocurrents in eliciting APs. Most importantly, the effect of temperature and light stimulation interaction in the membrane is greatly dependent on native voltage-gated channels.

## DISCUSSION

In this work, we have used the finite element method to address brain temperature changes caused by light stimulation in optogenetics and its effect in neuron firing. We found that temperature can increase about 2.6 $^{o}$C in one minute for blue light stimulation (20 mW of power, Figure 3c). A two-degree change in temperature, when applied to a model of a spontaneous firing neuron, caused a dramatic increase in firing frequency and change in action potential shape. Conversely, a 2 $^{o}$C-increase in temperature in a fast spiking interneuron network model of gamma oscillation produced a large increase in neuronal synchrony and in oscillation frequency. Moreover, the effect of channelrhodopsin-driven photocurrents on membrane potential is dramatically affected by temperature changes provoked by light stimulation itself, especially in the single-firing cell model.

In the context of optogenetics, the first study that addressed the interaction of light emanating from an optical fibre with brain tissue omitted absorption (Aravanis et al., 2007). Aravanis and colleagues argued that the effect of light (400-900 nm) absorption could be neglected when simulating light transmission in the brain (Aravanis et al., 2007). However, while absorption does not affect significantly the spatial computation of light intensity (as most of loss occurs through scattering), it is through absorption that heat is generated. In addition, we opt to

use the simpler Kubelka-Munk model for light transmission instead of a more accurate Monte Carlo method as the former generates values that approximate empirical results for short distances (~1 mm) (Aravanis et al., 2007; Dzimbeg-Malcic, Barbarić-Mikočević & Itrić, 2010).

Our bio-heat transfer results corroborate with a recent study by Stujenske and others (Stujenske, Spellman & Gordon, 2015). These authors were the first to explore heat generation by light in optogenetic experiments and compare simulations with empirical measurements. Our work, instead, explore the effect of bio-heat transfer in neurons and networks. Our simulations, however, have a few differences compared to the study by Stujenske and colleagues (Stujenske, Spellman & Gordon, 2015). For instance, the authors used light absorption and scattering coefficients obtained from human brain tissue interpolated from different wavelengths while here we employ coefficients obtained from rodent brains in specific wavelengths used in optogenetic experiments (Bernstein et al., 2008; Stujenske, Spellman & Gordon, 2015). Besides, we have calculated temporo-spatial photon flux in brain tissue. Ultimately, photon flux determines the opening of channelrhodopsin pores and these values could be directly used for simulation of channelrhodopsin activation (Zhang et al., 2015).

We used homogeneous absorption coefficients for a given wavelength but it is clear from optical measurements that light is unevenly absorbed in the brain (Jacques, 2013). Thus, temperature can also increase unevenly based on anisotropic absorption coefficients. Besides, blood vessels are not homogeneously distributed in all brain regions; therefore, spatial differences in temperature buffering will further complicate the network effect of heat generation by optical stimulation. In other words, the effect of increase in temperature in optogenetic experiments will depend on region, neuron type and connections and can significantly affect neuronal processing. Minimizing stimulation time may help to prevent unwanted heat effects in neuronal function. In experiments where long stimulation times are desirable, step-function opsins (Berndt et al., 2009) may be the tool of choice for preventing heat related changes in firing and behavior.

The temperature effect in the gating of voltage dependent channels is classically modelled by using an empirical factor ($Q_{10}$) to multiply rate constants (incorporating temperature dependence to the classical Hodgkin and Huxley formalism) (Thompson, Masukawa & Prince, 1985). In addition, ion reversal potentials in semipermeable membranes are directly proportional to temperature. We simulated the effect of a 2 °C change in a classical model of interneuron network gamma (ING) oscillation (Wang & Buzsáki, 1996). The idea that gamma oscillation arises from interaction of fast spiking interneurons originated from slice and modelling studies (Whittington, Traub & Jefferys, 1995; Wang & Buzsáki, 1996) and it was demonstrated by a highly influential optogenetics study (Cardin et al., 2009). Cardin and colleagues elicited gamma

oscillation in the neocortex by rhythmical optical stimulation of cells expressing the enzyme Cre recombinase (and channelrhodopsin) in a Parvalbumin-Cre animal (Cardin et al., 2009). To generate gamma oscillations, the authors optically stimulated neurons at the same frequency as the recorded local field potential (Cardin et al., 2009). It is known that rhythmical stimulation is likely to interfere with the local field potential recording due to the optoelectric effect (Mikulovic et al., 2016). However, the effect of temperature caused by optical stimulation in network responses is largely unexplored. Parvalbumin is especially found in soma targeting fast spiking interneurons (but it is also found in several other types of interneurons) (Klausberger et al., 2005; Mikulovic et al., 2016). Using Wang and Buzsaki's model of ING (1996), we found that an increase of two degrees significantly organizes the inhibitory neuron network. At 39 °C, firing in gamma can be observed in less than 50 ms from the simulation onset (when firing of individual neurons is random) while at 37 °C, that network takes almost 5 times longer to organize its spikes at gamma frequency. Also, network firing frequency increases in several Hz. Changes in gamma oscillation frequency by temperature has been observed experimentally (Leão, Tan & Fisahn, 2009), and as the increase in temperature depends on the proximity of targeted neurons to the optical fibre, light stimulation could generate small networks that oscillate incoherently from non-heated networks and this effect is not directly associated to opsin expression.

Temperature affects the transfer function of a neuron according to the diversity of ion channels in a given neuron (Cao & Oertel, 2005). For that reason, while some neuron types increase spontaneous firing, other populations may become quiet when temperature is changed (Kim & Connors, 2012). Most importantly, changes in temperature and native channels may hinder optogenetic stimulation. Our optogenetics simulations using the bushy cell model showed that light pulses are unable to elicit spikes when the cell is heated to 39 °C. Bushy cells are known to express low threshold potassium channels (Kv1) (Rothman & Manis, 2003) and these channels prevent the firing of multiple APs in response to tonic currents (Couchman et al., 2011). Thus, accelerating the opening of Kv1 channels could prevent spike generation by photocurrents. However, the interaction of channelrhodopsin photocurrents with native voltage-gated currents of a given cell is a subject largely explored, especially when changes in temperature caused by the light stimulation affects the gating dynamics of native channels. Future studies should assess the interaction of photocurrents with native voltage-gated currents and examine the effect of temperature.

## CONCLUSIONS

In conclusion,, we show that temperature increase caused by brain optical stimulation, with light intensities normally used in optogenetic experiments (Cardin et al., 2009; Adamantidis et al., 2011) can considerably affect neuron and network properties independently of opsin expression. Moreover, temperature can alter cellular responses to optical stimulation. As the usage of channelrhodopsin becomes widespread, studies tend to assume that optical stimulation elicits spiking activity without assessing cellular responses (Almada et al., 2018; Ahlbeck et al., 2018). Thus, whole cell current- and voltage-clamp assessment of the cell response to optical stimulation may still be necessary to determine optimal light stimulation protocols.

## ACKNOWLEDGEMENTS

## REFERENCES

Adamantidis AR., Tsai H-C., Boutrel B., Zhang F., Stuber GD., Budygin EA., Touriño C., Bonci A., Deisseroth K., de Lecea L. 2011. Optogenetic interrogation of dopaminergic modulation of the multiple phases of reward-seeking behavior. *The Journal of Neuroscience: The Official Journal of the Society for Neuroscience* 31:10829–10835. DOI: 10.1523/JNEUROSCI.2246-11.2011.

Adamantidis AR., Zhang F., de Lecea L., Deisseroth K. 2014. Establishing a Fiber-Optic-Based Optical Neural Interface. *Cold Spring Harbor Protocols* 2014:pdb.prot083337-pdb.prot083337. DOI: 10.1101/pdb.prot083337.

Adelsberger H., Grienberger C., Stroh A., Konnerth A. 2014. In Vivo Calcium Recordings and Channelrhodopsin-2 Activation through an Optical Fiber. *Cold Spring Harbor Protocols* 2014:pdb.prot084145-pdb.prot084145. DOI: 10.1101/pdb.prot084145.

Ahlbeck J., Song L., Chini M., Bitzenhofer SH., Hanganu-Opatz IL. 2018. Glutamatergic drive along the septo-temporal axis of hippocampus boosts prelimbic oscillations in the neonatal mouse. *eLife* 7. DOI: 10.7554/eLife.33158.

Akemann W., Mutoh H., Perron A., Rossier J., Knöpfel T. 2010. Imaging brain electric signals with genetically targeted voltage-sensitive fluorescent proteins. *Nature Methods* 7:643–649. DOI: 10.1038/nmeth.1479.

Almada RC., Genewsky AJ., Heinz DE., Kaplick PM., Coimbra NC., Wotjak CT. 2018. Stimulation of the Nigrotectal Pathway at the Level of the Superior Colliculus Reduces Threat Recognition and Causes a Shift From Avoidance to Approach Behavior. *Frontiers in Neural Circuits* 12:36. DOI: 10.3389/fncir.2018.00036.

Andersen P., Moser EI. 1995. Brain temperature and hippocampal function. *Hippocampus* 5:491–498. DOI: 10.1002/hipo.450050602.

Andrews R., Philips L. (eds.) 2005. *Laser beam propagation through random media*. SPIE Press.

Aravanis AM., Wang L-P., Zhang F., Meltzer LA., Mogri MZ., Schneider MB., Deisseroth K. 2007. An optical neural interface: in vivo control of rodent motor cortex with integrated

fiberoptic and optogenetic technology. *Journal of Neural Engineering* 4:S143. DOI: 10.1088/1741-2560/4/3/S02.

Balanis C. (ed.) 2012. *Advanced Engineering Electromagnetics.* John Wiley & Sons Inc.

Bernstein JG., Han X., Henninger MA., Ko EY., Qian X., Franzesi GT., McConnell JP., Stern P., Desimone R., Boyden ES. 2008. Prosthetic systems for therapeutic optical activation and silencing of genetically-targeted neurons. *Proceedings of SPIE--the International Society for Optical Engineering* 6854:68540H. DOI: 10.1117/12.768798.

Cao X-J., Oertel D. 2005. Temperature affects voltage-sensitive conductances differentially in octopus cells of the mammalian cochlear nucleus. *Journal of Neurophysiology* 94:821–832. DOI: 10.1152/jn.01049.2004.

Cardin JA., Carlén M., Meletis K., Knoblich U., Zhang F., Deisseroth K., Tsai L-H., Moore CI. 2009. Driving fast-spiking cells induces gamma rhythm and controls sensory responses. *Nature* 459:663–667. DOI: 10.1038/nature08002.

Couchman K., Garrett A., Deardorff AS., Rattay F., Resatz S., Fyffe R., Walmsley B., Leão RN. 2011. Lateral superior olive function in congenital deafness. *Hearing Research* 277:163–175. DOI: 10.1016/j.heares.2011.01.012.

Dzimbeg-Malcic V., Barbarić-Mikočević Ž., Itrić K. 2010. Kubelka-munk Theory in Describing Optical Properties of Paper (i)

Elwassif MM., Kong Q., Vazquez M., Bikson M. 2006. Bio-heat transfer model of deep brain stimulation-induced temperature changes. *Journal of Neural Engineering* 3:306–315. DOI: 10.1088/1741-2560/3/4/008.

Fenno L., Yizhar O., Deisseroth K. 2011. The development and application of optogenetics. *Annual Review of Neuroscience* 34:389–412. DOI: 10.1146/annurev-neuro-061010-113817.

Fitzhugh R. 1966. Theoretical Effect of Temperature on Threshold in the Hodgkin-Huxley Nerve Model. *The Journal of General Physiology* 49:989–1005.

Foutz TJ., Arlow RL., McIntyre CC. 2012. Theoretical principles underlying optical stimulation of a channelrhodopsin-2 positive pyramidal neuron. *Journal of Neurophysiology* 107:3235–3245. DOI: 10.1152/jn.00501.2011.

Hilscher MM., Leão KE., Leão RN. 2013. Synchronization through nonreciprocal connections in a hybrid hippocampus microcircuit. *Frontiers in neural circuits* 7:120. DOI: 10.3389/fncir.2013.00120.

Jacques SL. 2013. Optical properties of biological tissues: a review. *Physics in Medicine and Biology* 58:R37-61. DOI: 10.1088/0031-9155/58/11/R37.

Kim J., Connors B. 2012. High temperatures alter physiological properties of pyramidal cells and inhibitory interneurons in hippocampus. *Frontiers in Cellular Neuroscience* 6:27. DOI: 10.3389/fncel.2012.00027.

Klausberger T., Marton LF., O'Neill J., Huck JHJ., Dalezios Y., Fuentealba P., Suen WY., Papp E., Kaneko T., Watanabe M., Csicsvari J., Somogyi P. 2005. Complementary Roles of Cholecystokinin- and Parvalbumin-Expressing GABAergic Neurons in Hippocampal Network Oscillations. *The Journal of Neuroscience* 25:9782–9793. DOI: 10.1523/JNEUROSCI.3269-05.2005.

Knöpfel T., Lin MZ., Levskaya A., Tian L., Lin JY., Boyden ES. 2010. Toward the second generation of optogenetic tools. *The Journal of Neuroscience: The Official Journal of the Society for Neuroscience* 30:14998–15004. DOI: 10.1523/JNEUROSCI.4190-10.2010.

669 Leao KE., Leao RN., Sun H., Fyffe REW., Walmsley B. 2006. Hyperpolarization-activated
670 currents are differentially expressed in mice brainstem auditory nuclei. *The Journal of*
671 *physiology* 576:849–864. DOI: 10.1113/jphysiol.2006.114702.
672 Leao RN., Leao FN., Walmsley B. 2005. Non-random nature of spontaneous mIPSCs in mouse
673 auditory brainstem neurons revealed by recurrence quantification analysis. *Proceedings.*
674 *Biological sciences / The Royal Society* 272:2551–2559. DOI: 10.1098/rspb.2005.3258.
675 Leão RN., Tan HM., Fisahn A. 2009. Kv7/KCNQ channels control action potential phasing of
676 pyramidal neurons during hippocampal gamma oscillations in vitro. *The Journal of*
677 *Neuroscience: The Official Journal of the Society for Neuroscience* 29:13353–13364. DOI:
678 10.1523/JNEUROSCI.1463-09.2009.
679 Lerchner W., Corgiat B., Der Minassian V., Saunders RC., Richmond BJ. 2014. Injection
680 parameters and virus dependent choice of promoters to improve neuron targeting in the
681 nonhuman primate brain. *Gene Therapy* 21:233–241. DOI: 10.1038/gt.2013.75.
682 Madisen L., Mao T., Koch H., Zhuo J., Berenyi A., Fujisawa S., Hsu Y-WA., Garcia AJ., Gu X.,
683 Zanella S., Kidney J., Gu H., Mao Y., Hooks BM., Boyden ES., Buzsáki G., Ramirez JM.,
684 Jones AR., Svoboda K., Han X., Turner EE., Zeng H. 2012. A toolbox of Cre-dependent
685 optogenetic transgenic mice for light-induced activation and silencing. *Nature Neuroscience*
686 15:793–802. DOI: 10.1038/nn.3078.
687 Martina M., Schultz JH., Ehmke H., Monyer H., Jonas P. 1998. Functional and Molecular
688 Differences between Voltage-Gated K+ Channels of Fast-Spiking Interneurons and
689 Pyramidal Neurons of Rat Hippocampus. *The Journal of Neuroscience* 18:8111–8125.
690 Migliore M. 1996. Modeling the attenuation and failure of action potentials in the dendrites of
691 hippocampal neurons. *Biophysical Journal* 71:2394–2403.
692 Mikulovic S., Pupe S., Peixoto HM., Do Nascimento GC., Kullander K., Tort ABL., Leão RN.
693 2016. On the photovoltaic effect in local field potential recordings. *Neurophotonics* 3:015002.
694 DOI: 10.1117/1.NPh.3.1.015002.
695 Orazio S. (ed.) 2010. *Principles of lasers.* Springer.
696 Peatross J., Ware M. (eds.) 2015. *Physics of light and optics.* Brigham Young University.
697 Pennes HH. 1948. Analysis of tissue and arterial blood temperatures in the resting human
698 forearm. *Journal of Applied Physiology* 1:93–122. DOI: 10.1152/jappl.1948.1.2.93.
699 Rothman JS., Manis PB. 2003. The roles potassium currents play in regulating the electrical
700 activity of ventral cochlear nucleus neurons. *Journal of Neurophysiology* 89:3097–3113. DOI:
701 10.1152/jn.00127.2002.
702 Sadiku MNO. (ed.) 2010. *Elements of Electromagnetics.* Oxford University Press Inc.
703 Shapiro MG., Homma K., Villarreal S., Richter C-P., Bezanilla F. 2012. Infrared light excites
704 cells by changing their electrical capacitance. *Nature Communications* 3:736. DOI:
705 10.1038/ncomms1742.
706 Stujenske JM., Spellman T., Gordon JA. 2015. Modeling the Spatiotemporal Dynamics of Light
707 and Heat Propagation for In Vivo Optogenetics. *Cell Reports* 12:525–534. DOI:
708 10.1016/j.celrep.2015.06.036.
709 Thompson SM., Masukawa LM., Prince DA. 1985. Temperature dependence of intrinsic
710 membrane properties and synaptic potentials in hippocampal CA1 neurons in vitro. *The*
711 *Journal of Neuroscience: The Official Journal of the Society for Neuroscience* 5:817–824.
712 Vo-Dinh T. 2003. *Biomedical Photonics Handbook.* CRC Press.

Wang XJ., Buzsáki G. 1996. Gamma oscillation by synaptic inhibition in a hippocampal interneuronal network model. *The Journal of neuroscience: the official journal of the Society for Neuroscience* 16:6402–6413.

Weisstein E. 2016. Fourier Transform - Gaussian. From MathWorld - A Wolfram Web Resource.

Welch AJ., van Gemert MJ. (eds.) 2011. *Optical-Thermal Response of Laser-Irradiated Tissue*. Springer.

Whittington MA., Traub RD., Jefferys JG. 1995. Synchronized oscillations in interneuron networks driven by metabotropic glutamate receptor activation. *Nature* 373:612–615. DOI: 10.1038/373612a0.

Williams JC., Xu J., Lu Z., Klimas A., Chen X., Ambrosi CM., Cohen IS., Entcheva E. 2013. Computational optogenetics: empirically-derived voltage- and light-sensitive channelrhodopsin-2 model. *PLoS computational biology* 9:e1003220. DOI: 10.1371/journal.pcbi.1003220.

Yang L., Miklavcic SJ. 2005. Revised Kubelka-Munk theory. III. A general theory of light propagation in scattering and absorptive media. *Journal of the Optical Society of America. A, Optics, Image Science, and Vision* 22:1866–1873.

Zhang F., Tsai H-C., Airan RD., Stuber GD., Adamantidis AR., de Lecea L., Bonci A., Deisseroth K. 2015. Optogenetics in Freely Moving Mammals: Dopamine and Reward. *Cold Spring Harbor Protocols* 2015:pdb.top086330. DOI: 10.1101/pdb.top086330.

Zimmerman W. (ed.) 2004. *Process Modelling and Simulation with Finite Element Methods. Series A: Stability, Vibration and Control of Systems.*

## Figure Legends

**Figure 1. Light propagation properties when interacting with brain tissue. A.** Diagram showing a typical optic stimulation setup used in freely moving animals. The setup consists of a computer, a data acquisition (DAQ) board, and a laser source coupled to a fibre transmitting light to a target region into the mouse brain at a divergence angle ($\theta_{div}$) calculated using Eq. (21). **B.** Transversal electromagnetic fundamental propagation mode ($TEM_{00}$) of the laser source. **C.** Gaussian beam shape. **D.** 2D view of the geometric loss due to light dispersion in the tissue (conical shape) at a certain distance from the fibre tip. **E.** Flux of irradiated photons as a function of distance during 15, 60 and 100 ms light pulses considering a region of unit area. **F.** Wavelength shift during light propagation through different media.

**Figure 2. Scattering and absorption effects as light propagates into mouse brain tissue. A.** Light intensity *versus* penetration distance for 473 nm (blue) and 593 nm (yellow) wavelengths. At a distance $d$ = 0.4 mm from the fibre tip (dashed green line), a reference value for light intensity of 10 mW/mm$^2$ (solid green line; an approximate threshold for channelrhodopsin-2 activation) was chosen for blue and yellow light with (solid lines) and without (dashed lines) absorption. *Inset.* Distance in which light decays to 10 mW/mm$^2$ in simulations with and without absorption. **B.** Transmittance *versus* penetration distance for blue and yellow lights including scattering and absorption effects.

**Figure 3. Heat transfer simulations for blue and yellow light in mouse brain tissue.**

**A.** Temperature variations for 593 nm wavelength as a function of time for 1, 10, 20, 30, and 40 mW of continuous radiation. **B.** Temperature distribution in space for 593 nm and 473 nm. *Right. Top.* 2D Gaussian beam (*x*-*y*) for the top view and with $z \rightarrow 0$. *Bottom* 2D slice view (*z*-*x*) of the temperature distribution. **C.** Heat map for the temperature distribution (473 nm) as a function of frequency (1-40 Hz, bin size of 1 Hz) and duty cycle (1-100%, bin size of 10%) at 60 s of light radiation (10 μm from the fibre tip). The dashed black line shows a pulse width of 10 ms.

**Figure 4. A 2 °C raise in temperature increases the firing frequency of neurons in a network model of gamma oscillations. A.** Membrane potential of two neurons (gray and black traces – left) from a network of 100-interneuron network when simulation was executed with temperatures of 37 °C and 39 °C (red and dark red – right). **B.** Phase plots from one action potential of one interneuron at 37 °C and at 39 °C (black and dark red traces, respectively). **C.** Mean firing power spectrum density (see methods) of the 100 interneurons in the network at 37 °C and at 39 °C (black and dark red traces, respectively). **D.** Scatter plots showing the action potential firing of the gamma network at 37 °C (left) and at 39 °C (right).

**Figure 5. Synchrony is greatly increased in a gamma oscillation network model by a 2 °C raise in temperature. A.** Top, Normalised autocorrelograms of all 100 neurons in the network at 37 °C (left) and at 39 °C (right). Bottom, Normalised crosscorrelograms of all 100 neurons crosscorrelated with all 100 neurons in the network at 37 °C (left) and at 39 °C (right). **B.** Peak normalised correlation index between all 100 neurons when simulations were performed at temperatures of 37 °C (left) and 39 °C (right).

**Figure 6. Temperature changes caused by light absorption affects membrane response to photocurrents. A.** Membrane potential of a basket cell (BC) and a dorsal cochlear nucleus bushy cell (GBC) models to 10 mW-473 nm light pulses at 37 °C (top) and 39 °C (bottom). **B.** Temperature at 10 μm for 4 Hz stimulation (20 mW) for 10% (blue), 50% (magenta) and 90% (red) duty cycles (*inset* shows 0.5 s pulses with the three different duty cycles). **C.** BC and GBC responses for 10% duty cycle (4Hz) light pulses with fixed temperatures (37 °C – black and 39 °C – red) and when temperature raises (green) in response to light pulses (black trace in (b)). **D.** Action potential amplitude evolution in time of GBC model in response to light pulses in (**C**). The red square is the amplitude of the single AP the GBC model fired when temperature was set to 39 °C.

## Table 1(on next page)

Parameters used in scattering and absorption simulations

PeerJ Preprints | https://doi.org/10.7287/peerj.preprints.27248v1 | CC BY 4.0 Open Access | rec: 2 Oct 2018, publ: 2 Oct 2018

**Table 1. Parameters used in scattering and absorption simulations.**

| Parameters | Value | References |
|---|---|---|
| Fibre core radius ($r$) | 0.2 mm | (BFL48-400, Thorlabs) |
| Fibre numerical aperture ($NA$) | 0.48 | (BFL48-400, Thorlabs) |
| Fibre core refractive index ($n_1$) | Blue light: 1.4644<br>Yellow light: 1.4587 | (BFL48-400, Thorlabs) |
| Scattering coefficient ($\mu_s$) | Blue light: 10.0 $mm^{-1}$<br>Yellow light: 9.0 $mm^{-1}$ | (Aravanis et al., 2007; Bernstein et al., 2008) |
| Absorption coefficient ($\mu_a$) | Blue light: 0.070 $mm^{-1}$<br>Yellow light: 0.027 $mm^{-1}$ | (Aravanis et al., 2007; Bernstein et al., 2008) |
| Laser input power ($P$) | 20 mW | |
| Laser coupling fraction ($\eta$) | 1 or 100% | |

## Table 2(on next page)

Parameters and material properties used in heat transfer simulations

**Table 2. Parameters and material properties used in heat transfer simulations.**

| Parameters | Values | Reference |
|---|---|---|
| Refractive index of the tissue ($n_t$) | 1.36 (gray matter) | (Vo-Dinh, 2003) |
| Specific heat of the tissue ($C_p$) | 3650 J/kg°C | (Elwassif et al., 2006) |
| Density of the tissue ($\rho$) | 1040 kg/m$^3$ | (Elwassif et al., 2006) |
| Thermal conductivity of the tissue ($k$) | 0.527 W/m°C | (Elwassif et al., 2006) |
| Metabolic heat source ($H_m$) | 13698 W/m$^3$ | (Elwassif et al., 2006) |
| Blood density ($\rho_b$) | 1057 kg/m$^3$ | (Elwassif et al., 2006) |
| Blood perfusion ($\omega_b$) | 0.012 1/s | (Elwassif et al., 2006) |
| Specific heat of the blood ($C_b$) | 3600 J/kg°C | (Elwassif et al., 2006) |
| Temperature of the tissue ($T$) | 37 °C | (Elwassif et al., 2006) |
| Blood temperature ($T_b$) | 36.7 °C | (Elwassif et al., 2006) |
| Heat transfer coefficient ($h$) | 25 W/m$^2$ °C | |
| Standard deviations in $x$ and $y$ axis, ($\sigma_x$, $\sigma_y$) | 0.5 | |
| Reflection coefficient ($R$) | 0 | |

# Figure 1

Light propagation properties when interacting with brain tissue

**A.** Diagram showing a typical optic stimulation setup used in freely moving animals. The setup consists of a computer, a data acquisition (DAQ) board, and a laser source coupled to a fibre transmitting light to a target region into the mouse brain at a divergence angle ($\theta_{div}$) calculated using Eq. (21). **B.** Transversal electromagnetic fundamental propagation mode ($TEM_{00}$) of the laser source. **C.** Gaussian beam shape. **D.** 2D view of the geometric loss due to light dispersion in the tissue (conical shape) at a certain distance from the fibre tip. **E.** Flux of irradiated photons as a function of distance during 15, 60 and 100 ms light pulses considering a region of unit area. **F.** Wavelength shift during light propagation through different media

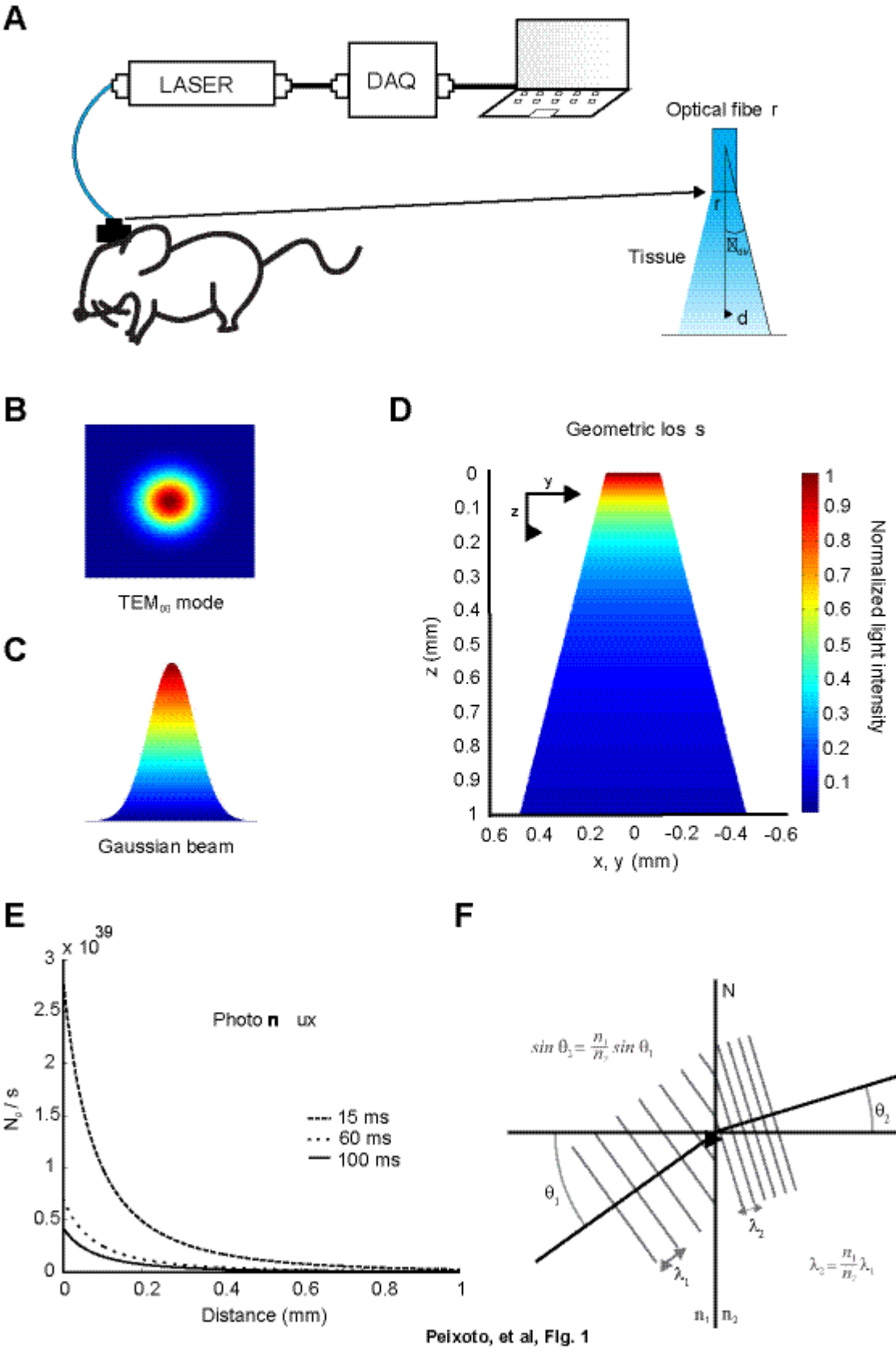


Peixoto, et al, Fig. 1

# Figure 2

Figure 2. Scattering and absorption effects as light propagates into mouse brain tissue.

**A.** Light intensity *versus* penetration distance for 473 nm (blue) and 593 nm (yellow) wavelengths. At a distance *d* = 0.4 mm from the fibre tip (dashed green line), a reference value for light intensity of 10 mW/mm$^2$ (solid green line; an approximate threshold for channelrhodopsin-2 activation) was chosen for blue and yellow light with (solid lines) and without (dashed lines) absorption. *Inset.* Distance in which light decays to 10 mW/mm$^2$ in simulations with and without absorption. **B.** Transmittance *versus* penetration distance for blue and yellow lights including scattering and absorption effects.

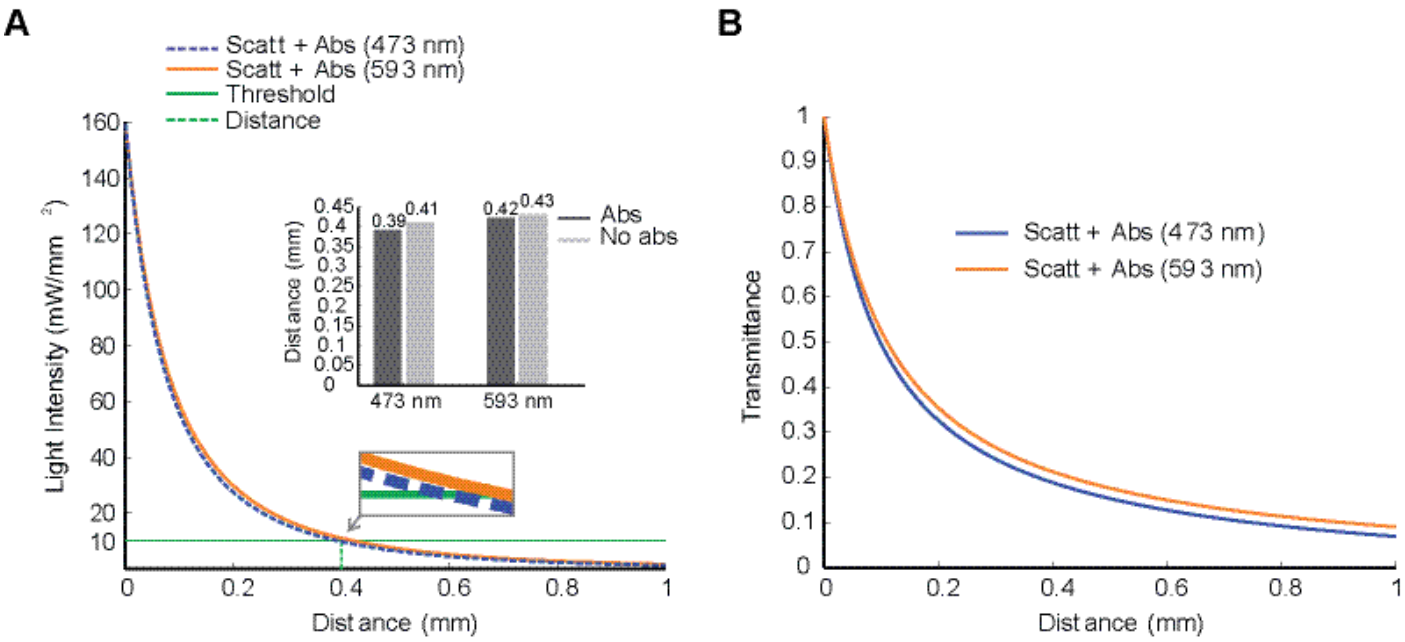


Peixoto et al, Figure 2

# Figure 3

Heat transfer simulations for blue and yellow light in mouse brain tissue.

**A.** Temperature variations for 593 nm wavelength as a function of time for 1, 10, 20, 30, and 40 mW of continuous radiation. **B.** Temperature distribution in space for 593 nm and 473 nm. *Right. Top.* 2D Gaussian beam (*x*-*y*) for the top view and with $z \rightarrow 0$. *Bottom* 2D slice view (*z*-*x*) of the temperature distribution. **C.** Heat map for the temperature distribution (473 nm) as a function of frequency (1-40 Hz, bin size of 1 Hz) and duty cycle (1-100%, bin size of 10%) at 60 s of light radiation (10 µm from the fibre tip). The dashed black line shows a pulse width of 10 ms.

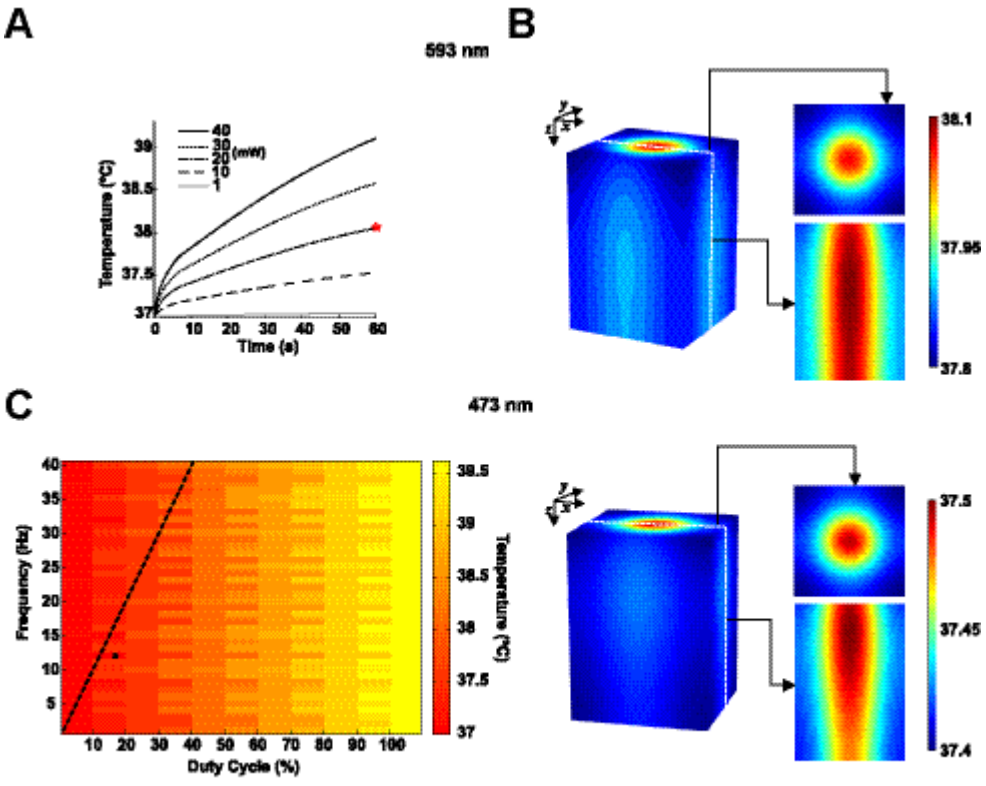


Peixoto et al, Figure 3

# Figure 4

A 2 °C raise in temperature increases the firing frequency of neurons in a network model of gamma oscillations.

**A.** Membrane potential of two neurons (gray and black traces – left) from a network of 100-interneuron network when simulation was executed with temperatures of 37 °C and 39 °C (red and dark red – right). **B.** Phase plots from one action potential of one interneuron at 37 °C and at 39 °C (black and dark red traces, respectively). **C.** Mean firing power spectrum density (see methods) of the 100 interneurons in the network at 37 °C and at 39 °C (black and dark red traces, respectively). **D.** Scatter plots showing the action potential firing of the gamma network at 37 °C (left) and at 39 °C (right).

PeerJ Preprints | https://doi.org/10.7287/peerj.preprints.27248v1 | CC BY 4.0 Open Access | rec: 2 Oct 2018, publ: 2 Oct 2018

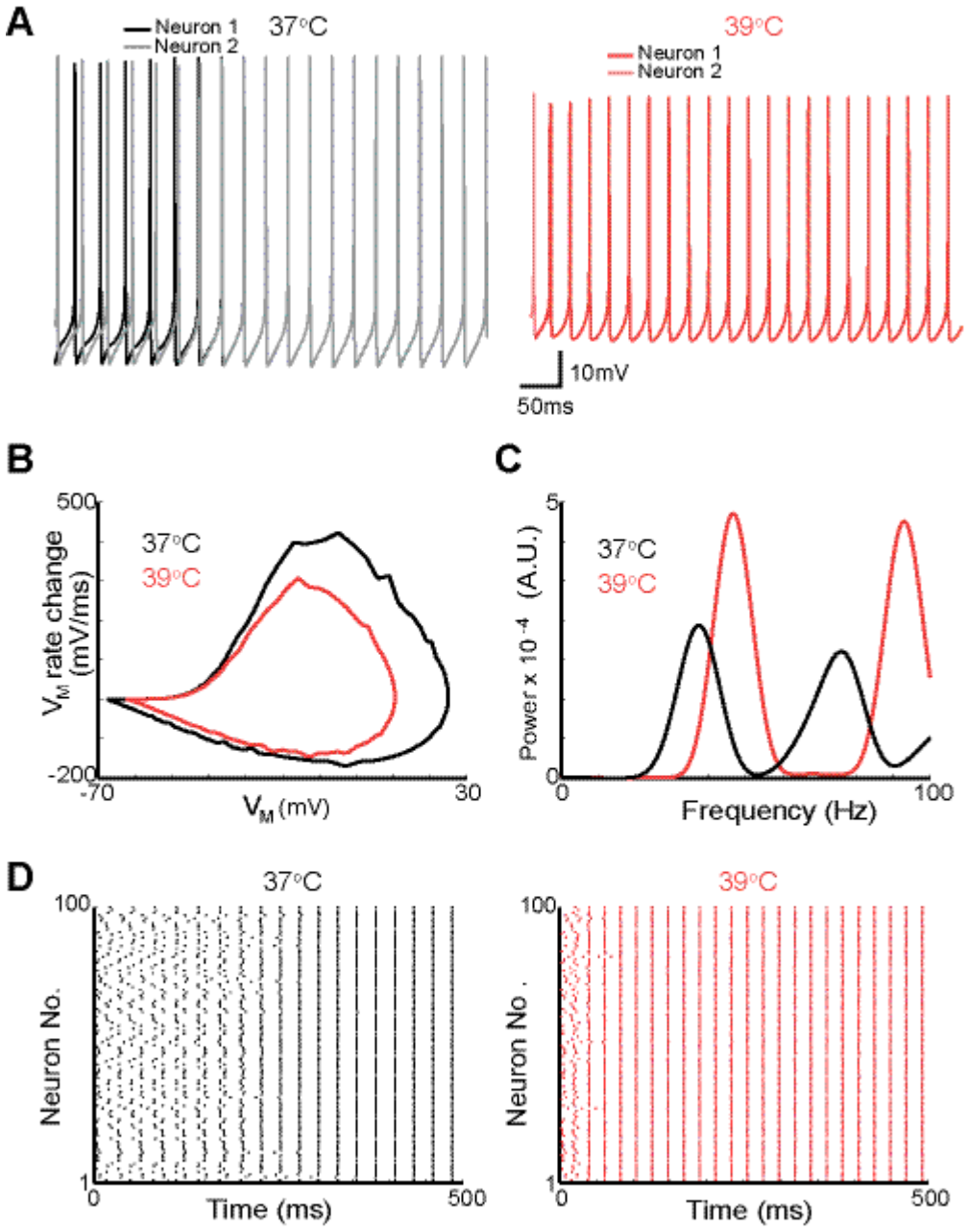


Peixoto et al, Figure 4

# Figure 5

Synchrony is greatly increased in a gamma oscillation network model by a 2 °C raise in temperature.

**A.** Top, Normalised autocorrelograms of all 100 neurons in the network at 37 °C (left) and at 39 °C (right). Bottom, Normalised crosscorrelograms of all 100 neurons crosscorrelated with all 100 neurons in the network at 37 °C (left) and at 39 °C (right). **B.** Peak normalised correlation index between all 100 neurons when simulations were performed at temperatures of 37 °C (left) and 39 °C (right).

PeerJ Preprints | https://doi.org/10.7287/peerj.preprints.27248v1 | CC BY 4.0 Open Access | rec: 2 Oct 2018, publ: 2 Oct 2018

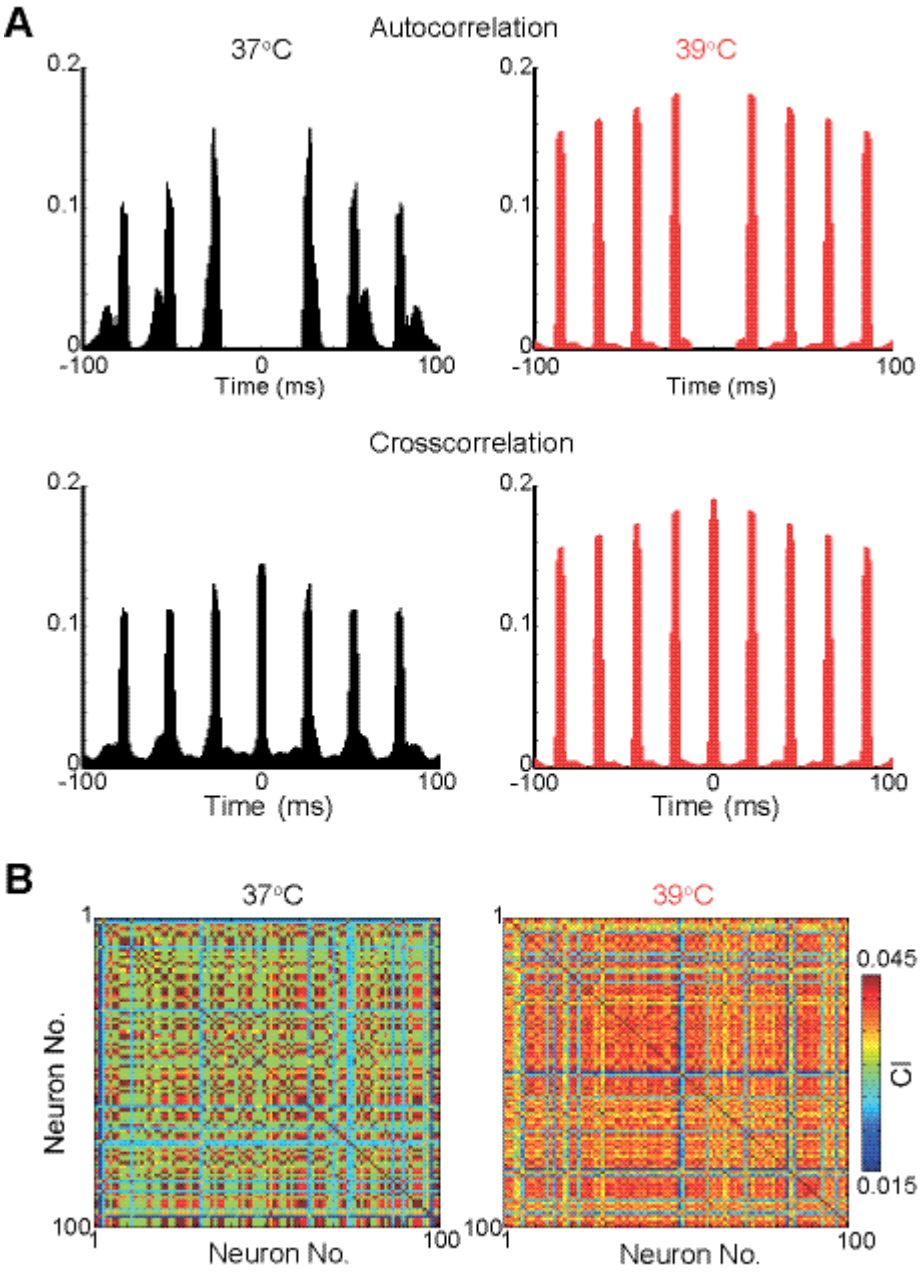


Peixoto et al, Figure 5

# Figure 6

Temperature changes caused by light absorption affects membrane response to photocurrents.

**A.** Membrane potential of a basket cell (BC) and a dorsal cochlear nucleus bushy cell (GBC) models to 10 mW-473 nm light pulses at 37 °C (top) and 39 °C (bottom). **B.** Temperature at 10 µm for 4 Hz stimulation (20 mW) for 10% (blue), 50% (magenta) and 90% (red) duty cycles (*inset* shows 0.5 s pulses with the three different duty cycles). **C.** BC and GBC responses for 10% duty cycle (4Hz) light pulses with fixed temperatures (37 °C – black and 39 °C – red) and when temperature raises (green) in response to light pulses (black trace in (b)). **D.** Action potential amplitude evolution in time of GBC model in response to light pulses in (**C**). The red square is the amplitude of the single AP the GBC model fired when temperature was set to 39 °C.

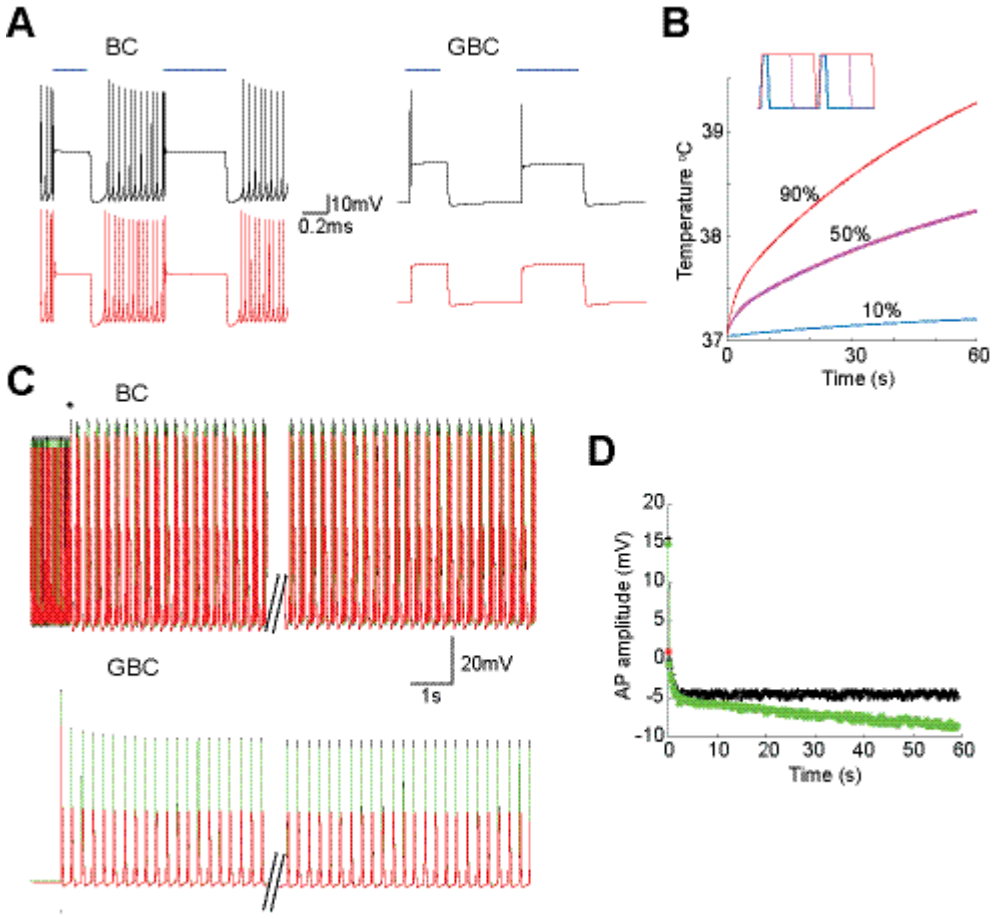


Peixoto et al, Figure 6